Polyhedron 249 (2024) 116789

Contents lists available at ScienceDirect

Polyhedron

journal homepage: www.elsevier.com/locate/poly

New α-keto acid-derived hydrazone ligands and their reaction with the $\{Re(CO)_3\}^+$

Aida Lorenzo [a,b], Saray Argibay-Otero [a,b,*], Carlos Platas-Iglesias [c], Ezequiel M. Vázquez-López [a,b]

[a] Universidade de Vigo, Departamento de Química Inorgánica, Facultade de Química, 36310 Vigo, Spain
[b] Metallosupramolecular Chemistry Group, Galicia Sur Health Research Institute (IIS Galicia Sur), SERGAS-UVIGO, Galicia, Spain
[c] Universidade da Coruña, Centro Interdisciplinar de Química e Bioloxía (CICA) and Departamento de Química, Facultade de Ciencias, A Coruña, Galicia, Spain

ARTICLE INFO

Keywords:
Rhenium
Hydrazone
α-ketoacid
Carbonyl complexes

ABSTRACT

Two hydrazone ligands derived of phenylglyoxylic acid (HL^1) and 4-hydroxyphenylpyruvic acid (HL^2) were synthesized and their zwitterionic structures were determined by X-ray diffraction. The rhenium(I) complexes of formula $[ReCl(HL^n)(CO)_3]$ were obtained by reaction of the ligands with $[ReCl(CH_3CN)_2(CO)_3]$. The formation of the hydazonate complexes were also achieved. In the case of HL^1 the trimetic complex $[Re_3(L^1)_3(CO)_9]$ was isolated by using a basic medium. On the other hand, from storage of a solution of the $[ReCl(HL^2)(CO)_3]$ complex, crystals of the $[Re_2(L^2)_2(CO)_6]$ dimer could be obtained for their structural analysis by X-ray diffraction. The study of the crystalline structures is included. The coordination geometry around rhenium(I) can be described as octahedral with three carbon atoms in *fac* configuration. In all complexes a five-membered chelate ring is formed including two nitrogen atoms from the hydrazone chain and the pyridine group. In the mononuclear complexes the carboxylic group does not participates in the coordination but acts as a bridge to form the polynuclear compounds. The coordination mode of the ligands in all the complexes could be corroborated by comparative studies of the experimental and calculated (DFT) IR spectra.

1. Introduction

The α-keto acids are of major importance in intermediary metabolism and as components of the Krebs cycle and they are used as model substrates of enzymes and in the development of enzyme inhibitors [1,2]. In particular, 4-Hydroxyphenyl pyruvic acid (=4-HPA, Scheme 1) is an important product of tyrosine metabolism in transitory and hereditary tyrosinemia [3]. Its determination in biological fluids contributes to obtain a precocious and valuable picture of the amino acid metabolic disease [4]. On the other hand, phenylglyoxylic acid (=PGA) together with alanine are the breakdown products of phenylalanine, and is therefore useful in the diagnosis of phenylketonuria (deficiency of this amino acid) [5]. As the main metabolite of styrene, it can be used for quantification in urine [6,7].

The hydrazone moiety ($R_2C = N\text{-}NH_2$) confers great versatility when designing ligands [8]. The synthesis is simple and its applications are known to be of interest in different fields. Spectrophotometric determination of cations is the most common application of these systems, which have proven to be able to detect different metal ions. Hydrazones have been also incorporated into gels as drug delivery systems for medical applications [9]. In addition, there are multiple applications in the field of pharmacological chemistry: the antibacterial Nifuroxazide [10] and isonicotinic acid hydrazide are both currently in clinical use, the latter for the treatment of tuberculosis [11]. The cytotoxic behaviour of these compounds is also noteworthy, as they show selectivity for different cancer cell lines [12], among which their high activity against breast cancer is remarkable [13].

In many cases, the biological behaviour of hydrazones is related to their coordination to a metal centre, often increasing the activity of the complex with respect to free ligands [14,15]. In the particular case of rhenium, there are numerous reports on active complexes with hydrazone ligands and in some cases interesting biological properties have been described [16,17]. This metal is also important because it is the main surrogate in the design of ^{99m}Tc complexes as radiopharmaceuticals for diagnostic imaging using the single photon emission computed tomography (SPECT) technique. The *fac*-$\{^{99m}Tc(CO)_3\}^+$ coordination

* Corresponding author at: Universidade de Vigo, Departamento de Química Inorgánica, Facultade de Química, 36310 Vigo, Spain.
E-mail address: saargibay@uvigo.gal (S. Argibay-Otero).

https://doi.org/10.1016/j.poly.2023.116789
Received 3 October 2023; Accepted 8 December 2023
Available online 19 December 2023

centre offers important advantages when designing a radiopharmaceutical because of its biocompatibility. The hydrophobic character of the carbonyl groups facilitates its biodistribution, as well as conferring a high configurational robustness and inertness [18].

The $\{M(CO)_3\}^+$ (M = Tc, Re) complexes are especially stabilised by aromatic nitrogen atoms such as those of imidazole or pyridine [19,20]. For instance, Ramesh *et al* [21] reported interesting tridentate pyridin-2-yl hydrazine Re/^{99m}Tc chelates showing strong binding affinity to oestrogen receptor. In this work, we report new ligands obtained by condensation between 2-hydrazino pyridine and pyruvic acid derivatives. This ligand family is very versatile, as it can be readily functionalised by varying the substituent R of the precursor (Scheme 1). This new design is expected to afford coordination to the metal via the hydrazine and pyridyl N atoms, forming a five-membered chelate that has been previously observed for structurally related systems [22]. However, we will show that the reaction conditions and the nature of the substituent of the pyruvic acid moiety plays a critical role on the final structure of the complex, which goes from the expected mononuclear complexes **1A** and **1C** (Scheme 1) to di- and tri-nuclear assemblies. The complexes were characterized using different spectroscopic techniques, single-crystal X-ray crystallography and DFT calculations.

2. Results and discussion

2.1. Synthesis and spectroscopic characterization

In the design of the **HL^1** and **HL^2** ligands (Scheme 1, top) a carboxylate arm was included at the hydrazone position (*C*2). The carboxylate group can be used to couple the $\{M(CO)_3\}$ (M = Tc, Re) moiety to biomolecules or targeting units by simple carboxyl group coupling reactions. Furthermore, this arm potentially increases the denticity of the ligands if they are confronted with another coordination core. The PGA and 4-HPA precursors were chosen because of their interest in amino acid metabolism (as mentioned above); in addition, the first is susceptible to derivatization if necessary.

The ligands **HL^1** and **HL^2** (Scheme 1) were obtained by reaction of the corresponding commercially available glyoxylic derivative (PGA or 4-HPA) and 2-hydrazino pyridine (synthesis details are collected in the Supplementary material). The **HL^2** ligand was isolated in a modest yield (46 %) when compared to **HL^1** (88 %). This is probably due to the predominant enol form of 4-HPA α-keto acid as illustrated in the Scheme 2, which is in fact the only tautomer observed in the ^{1}H NMR spectrum in DMSO-d_6 of 4-HPA (Supplementary material 5.2). This tautomeric form has been described to prevail in neutral media, while when buffered at pH 6 the equilibrium is reversed. However, we did not observe an improvement in the performance of the reaction done in the presence of an acid. The possible causes have not been studied but, among other factors, the acidic medium can increase the hydrated form [23] or produce the protonation of the hydrazine reagent.

The formation of the ligands was confirmed by analysis of the ^{1}H NMR, IR and MS-ESI spectra, and their purity was confirmed by elemental analysis. The IR spectra display a set of bands corresponding to the ν(C═O) and ν(C═N) stretching modes of the carboxylic, pyridine and hydrazine groups, which are observed around 1650 and 1550 cm^{-1},

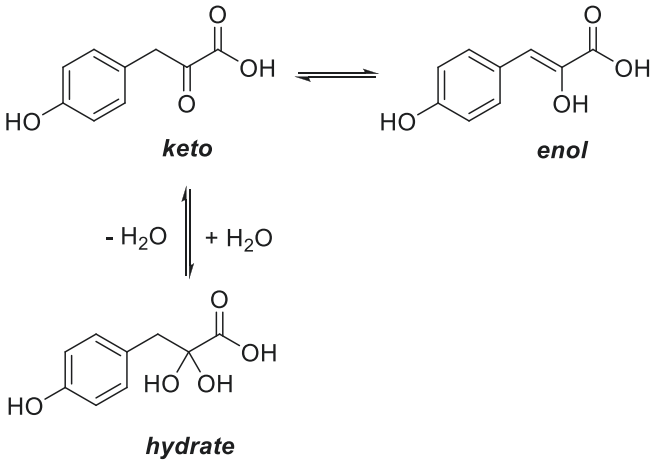

Scheme 2. Keto-enolic tautomerism and hydration of 4-HPA.

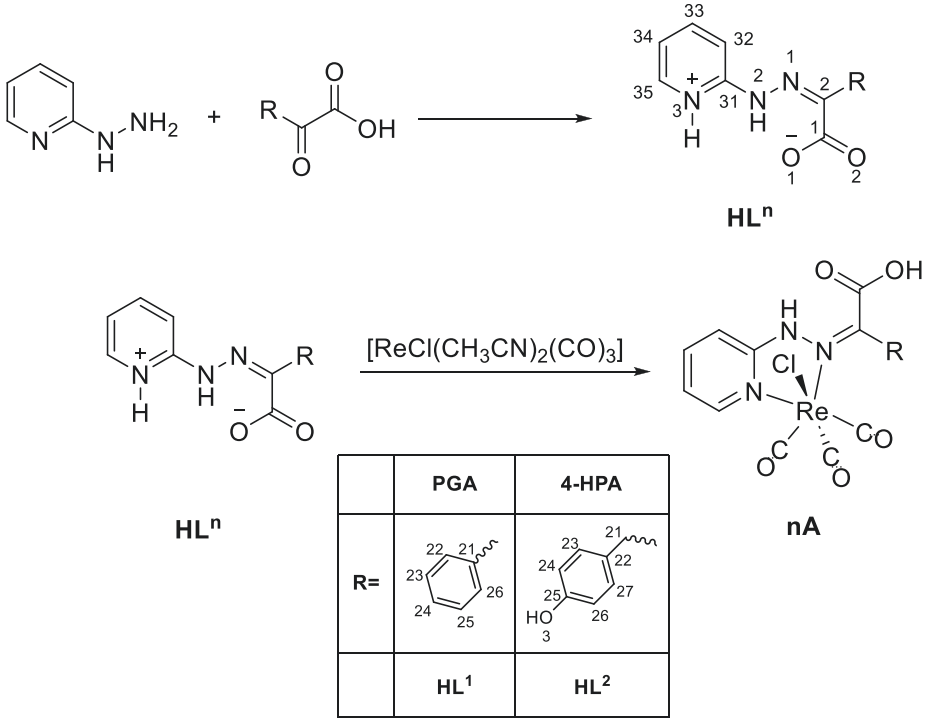

Scheme 1. Synthesis of the ligands HL$^{1\text{-}2}$ and complexes **1A** and **2A**.

respectively. The ^{1}H NMR spectra of DMSO-d_6 solutions show a signal around 12.30 ppm due to the N2-H hydrazine proton. The signal of the carboxylic proton is not observed, in agreement with the zwitterionic nature of these compounds by transfer of the carboxylic proton to the pyridine group, as the X-ray diffraction studies proved in the solid state (*vide infra*).

The rhenium(I) complexes of stoichiometry [ReCl(HL)(CO)$_3$] (**1A** and **2A**) were obtained as solvates after refluxing *fac*-[ReCl(CH$_3$CN)$_2$(CO)$_3$] with the corresponding ligand (Scheme 2, bottom). The proposed stoichiometry of **1A**·$^1/_3$CHCl$_3$ and **2A**·H$_2$O was confirmed by elemental analysis and, in the case of **1A**, the solvent could also be quantified through integration of the ^{1}H NMR spectrum. The mass spectra recorded using the electrospray technique showed peaks due to the $|M-Cl|^+$ entities, in which the chloride ligand is lost. This behaviour has been previously observed in rhenium(I) complexes containing Schiff bases such as acyl-hydrazones or thiosemicarbazones [24]. The *fac* configuration of the carbonyl groups in the $\{Re(CO)_3\}^+$ moiety was confirmed by observation of three strong/very strong bands in the 1880–2030 cm^{-1} range of the IR spectra (occasionally, the two lowest energy bands collapse). The bands due to the carboxylate and hydrazone groups ν(C═O) and ν(C═N) stretching modes observed in the region 1700–1450 cm^{-1} are shifted to higher wavenumbers with respect to the free ligands.

The ^{1}H NMR spectra of freshly prepared solutions of **1A** and **2A** complexes in acetone-d_6 and DMSO-d_6 display two sets of signals for most protons (Supplementary material 5.3 and 5.4). The spectra evolve with time when the solutions are exposed to air as the amount of water increases, observing the signals due to the minor species decreasing as their experience shifts to higher fields. However, the invariance of the ^{1}H NMR spectrum of **2A** in CD$_3$OD with time demonstrates its stability in this solvent. The minor species of **2A** shows a signal around 13.9 ppm assigned to the hydrazine N2–H proton, while this signal is observed at 10.9 ppm for the major species (in acetone-d_6). The latter chemical shift is consistent with the N2–H group establishing a hydrogen bond with the neighbouring carboxylate, as observed in the X-ray structure of the free ligand (*vide infra*). Thus, we tentatively assign the signals of the minor species to the complex having a protonated carboxylate and the major signals to the deprotonated form. The carboxylic acid proton dissociates in acetone-d_6 and DMSO-d_6 solution as the amount of water increases, and thus the population of the latter species is increased.

The chemical shift of the N2-H signal in hydrazone and acyl-hydrazone rhenium complexes respect to the free ligand has been related with the participation of the N—H group in the chelate ring. Often, the participation in the five-membered chelate ring produces a deshielding of this signal by more than 1 ppm [22,25]. However, in the present case, the formation of the complex causes a significant shielding of this signal of ~ 0.6 ppm ppm (in DMSO-d_6). This is most likely related to the relative strengths of the hydrogen-bond involving the N2-H group and the neighbouring carboxylate in the free ligand and in the complex.

The solutions of the [ReCl(HL)(CO)$_3$] complexes in acetone-d_6 and DMSO-d_6 are stable over time, as demonstrated by their ^{1}H NMR spectra. However, when a solution of **2A** in methanol was stored a r.t., crystals of the dimeric complex [Re$_2$(L^2)$_2$(CO)$_6$], **2B**, were isolated and characterized using X-ray diffraction (*vide infra*). The ^{1}H NMR spectrum of **2B** recorded in DMSO-d_6 (Fig. 1 or Supplementary material 5.3) indicates the presence of a single species in solution, in contrast to **2A**. The number of signals is compatible with the formation of a centrosymmetric dimer, as suggested by the solid state structure. The signals of the benzylic protons (–CH$_2$-) are observed as AB spin systems for the two species of **2A** in the range 3.95–4.30 ppm. The spectrum of **2B** shows a well-defined AB spin system (^2J = 16.0 Hz) with signals at 3.68 and 4.49 ppm. One of the benzyl protons is likely shielded by the carboxylate group, as it lies 2.12 Å above the plane defined by the carboxylate group in the X-ray structure.

Noteworthy, the formation of the dinuclear complex **2B** implies the deprotonation of the ligand HL^2 and the substitution of a chloride ligand by the oxygen carboxylate of the partner unit. Thus, we carried out the reaction of HL^2 with *fac*-[ReCl(CH$_3$CN)$_2$(CO)$_3$] in THF in the presence of NEt$_3$, which afforded a solid that appears to be a complex mixture of different species, as evidenced by the ^{1}H NMR spectrum recorded in DMSO-d_6 (Fig. 1). Analysing the ^{1}H NMR spectrum of the mixture, we can observe at least three sets of signals that do not match those detected

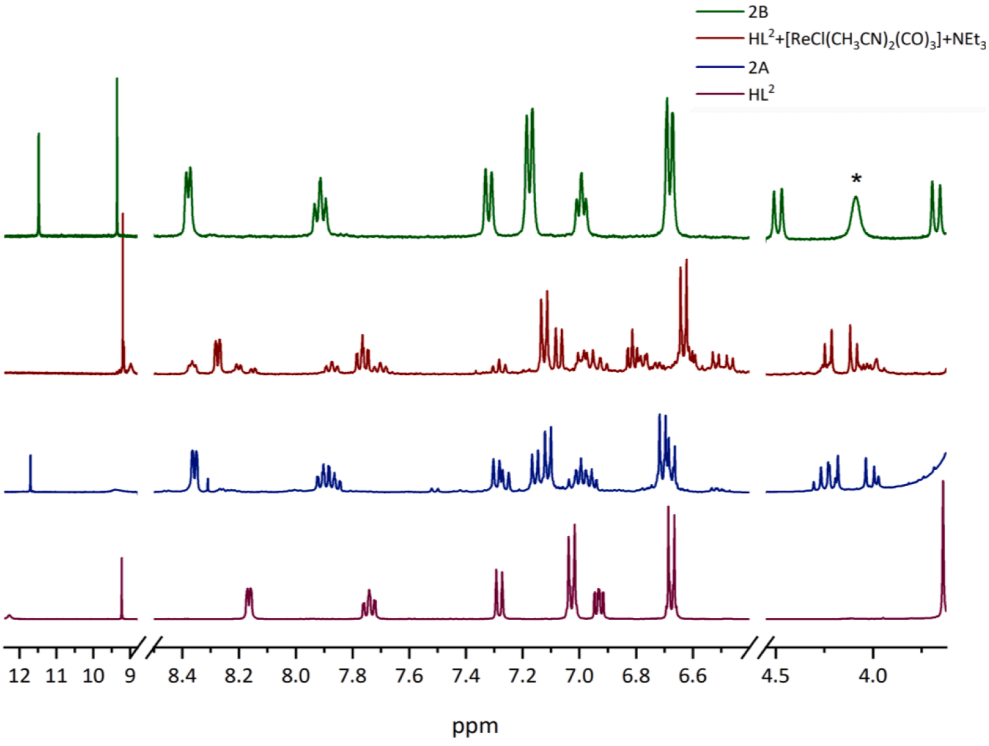

Fig. 1. Overlay of ^{1}H RMN spectra in DMSO-d_6 of **HL^2**, **2A**, HL^2 + [ReCl(CH$_3$CN)$_2$(CO)$_3$] + NEt$_3$ and, **2B**.

in spectra of the characterized complexes **2A** and **2B**. However, this does not rule out the presence of dimeric species in the crude, as we have previously reported that the arrangement of the ligands around the metal core gives rise to multiple different structures [26]. The reaction performed under the same conditions with HL^1 allowed us to isolate the trinuclear complex **1C**, as demonstrated by ^{1}H NMR spectroscopy (Scheme 3, see also Supplementary material 5.3). As observed for compound **1A**, the aromatic ^{1}H signals of **1C** experience important shifts with respect to the free ligand $\mathbf{HL^1}$, up to ≈0.3 ppm. However, we note that the ^{1}H NMR spectrum of **1C** recorded in DMSO-d_6 changes with time over a period of a few days, a behaviour that may be related to the dissociation of the trinuclear structure due to solvent coordination and/or formation of species with different nuclearity. On the other hand, the IR bands in the area attributed to the carbonyl ligands present specific patterns depending of the nuclearity of the complex formed. This aspect is discussed with the theoretical structure calculations (*vide infra*).

The trinuclear nature of the **1C** complex could be proved, in addition to the X-ray diffraction study of two different samples (see Experimental section), by ESI-MS and the comparative study of experimental and theoretical IR spectra (*vide infra*). The mass spectrum showed the peak corresponding to the $|M + H|^+$ entity low intensity,with the $|M/3 + H|^+$ species being the base-peak. This finding it is not surprising because it has been observed in other polymeric rhenium complexes, [27] which were found to be unstable under the ionization conditions used by the electrospray technique.

2.2. Crystal structures

The molecular structures of $\mathbf{HL^1}$ and $\mathbf{HL^2}$ (Fig. 2) were determined by X-ray diffraction using single crystals obtained by slow evaporation of DMSO or THF solutions, respectively. The models obtained showed reasonable residual factors and gave meaningful structural data (Table 1).

The structures of the type of ligands included in this work have been scarcely explored. Most of the compounds deposited in the CCDC database derived from 2-hydrazinopyridine are cyclic compounds resulting from the condensation with dicarbonyl derivatives,[28] with no pyruvic acid derivatives reported to date. Furthermore, only one structure of a metal (tin) complex with a hydrazone derived from 2-hydrazinopyridine has been reported.[29] Structures of complexes with related ligands derived from picolinaldehydes (or ketones) and oxoacetates after reduction of the imine bond are more common. The examples reported include some complexes of copper (QOWWOP, QOWWUV, QOWXAC [30], AHAWEN, AHAWIR [31]) and cadmium (BANQEO [32], RISMEO [33]), where the ligand presents a κ^2-N_{py},N coordination mode, a cobalt compound (VAVFAA [34]) where the carboxylate group also participates in coordination (κ^3-N_{py},N,O) and a dimeric zinc species NEWQOX [35] where the carboxylate group acts as a bridge between the metal centers (μ-1κ^3 N_{py},N,O:2κO).

The structures of both ligands present a strong intramolecular interaction involving the N2-H group and the carboxylate oxygen O1 forming a six-membered ring (*S(6)*).[36] This interaction has a stabilizing effect of the *Z* configuration on the N1-C2 bond. The *E* configuration of this bond is ussually observed for hydrazones derived from aldehydes [25] or methyl ketones (XALDET [37]). Both conformational isomers were however observed when one of the ketone substituents is a phenyl group (LILJOH/LILJUN [38]).

The rings connected by the hydrazineylidene group are practically coplanar for $\mathbf{HL^1}$ (10°) and perpendicular for $\mathbf{HL^2}$ (85°). The C1–O2 and C1-O1 bond distances point to π delocalization due to the deprotonated carboxylic group and, while the C2–N1 bond distance suggests a double bond character, some π delocalization along the hydrazone chain is likely also present [39].

The main intermolecular interactions present in the crystal of $\mathbf{HL^1}$ associate two molecules in centrosymmetric dimers (Fig. 2a). The pyridinium and hydrazinic N—H groups act as H-donors interacting with the carboxylate oxygen of the partner molecule to form several rings. These interactions are also observed in the crystal of $\mathbf{HL^2}$·**THF**, but in addition the O—H group interacts with the carboxylate group (O3-H···O2) of a neighbour dimer, linking the dimers in chains running along the crystallographic a axis. The THF molecule, which exhibits 80/20 disorder, is hosted between the shackles of the chain (Fig. 2c).

An interesting aspect of all structures studied in this work is that the bond distances along the hydrazone arm are hardly modified with the metalation (**1A**) and deprotonation (**2B** and **1C**) respect to those observed in the free ligand. In complex **1A** (Fig. 3a), the proton is transferred to the carboxylic group as consequence of the rhenium coordination to the pyridine and azomethinic nitrogen atoms of $\mathbf{HL^1}$. The N atoms of the resulting five-membered chelate ring, the halogen atom and the three facial carbonyl groups complete the octahedral coordination geometry around the rhenium atom. As expected, the formation of the chelate ring with a *N*-Re-N angle of 75.53(13)° imposes the main distortion of the ideal geometry. The Re-Cl and Re-N distances are close to those found in Re(I) complexes of hydrazones and acylhydrazones showing κ^2-N,N coordination.[40] On the other hand, the carboxylic group does not participate in coordination, but maintains the intramolecular interaction with the hydrazone proton (N2-H···O2) observed in the free ligand. No significant effects are observed on the bond distances of the hydrazone group upon rhenium coordination. The molecules of **1A** are associated in chains running along the crystallographic a axis by intermolecular H-bonds involving the hydrazinic N—H and carboxylic O—H as donor groups and the chloride ligand as acceptor group (Fig. 4, top). The O1-H···Cl and N1-H···Cl interactions define a link to associate four molecules forming a the $R_4^4(12)$.

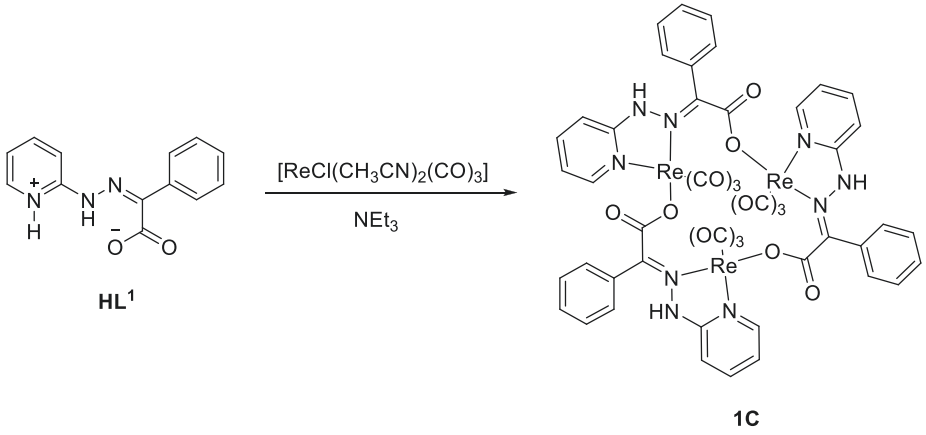

Scheme 3. Synthesis of the **1C** complex.

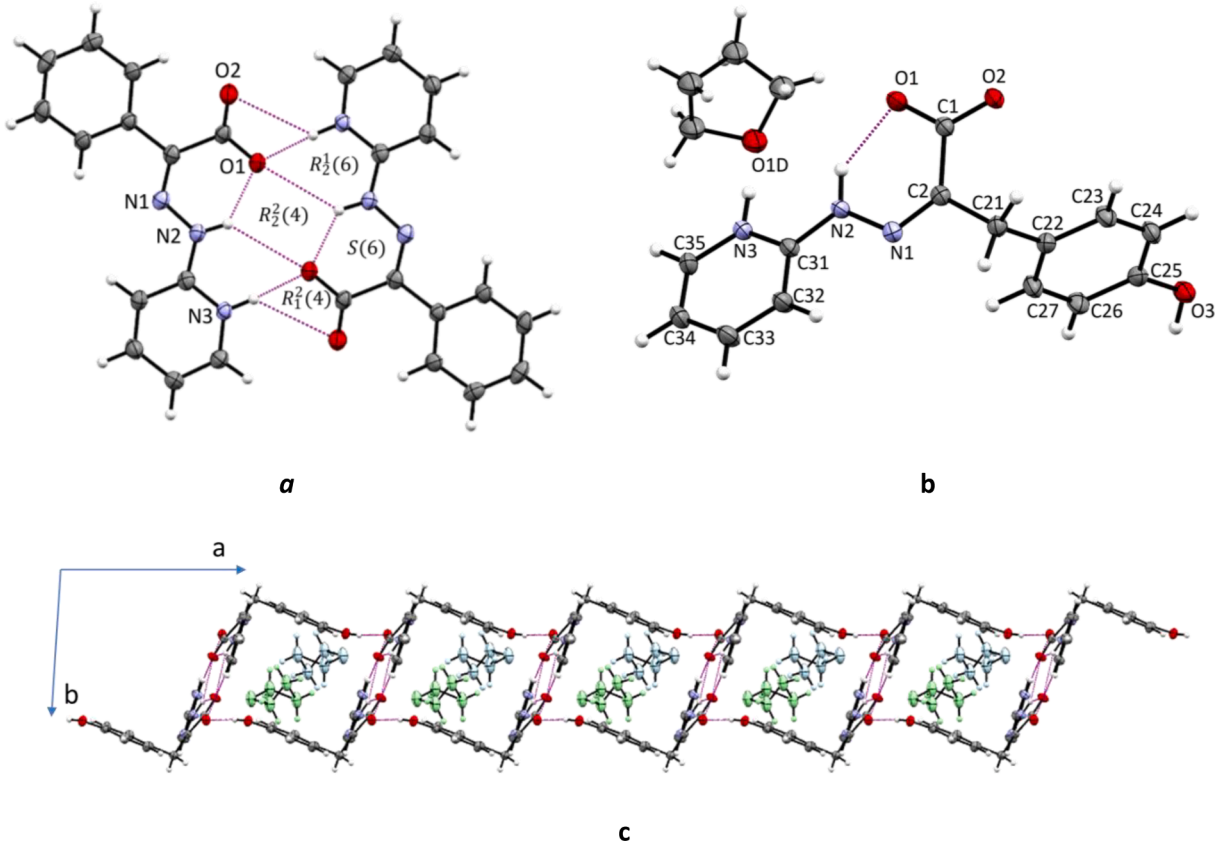

Fig. 2. Details of the crystal structures of HL^1 (a), describing the centrosymmetric dimer, the asymmetric unit in HL^2·THF, and the association of the ligand molecules, along crystallographic axis allows the guest THF (c). The disordered minority THF molecule is omitted for clarity.

Table 1
Selected bond distances and angles for the ligands **HL^1** and **HL^2** and their rhenium complexes.

Compound	**HL^1**	**HL^2·THF**	**1A**	**2B·2CH_3OH**	**1C·2DMSO**[(a)]
X=			Cl	O(1)	O(1)
Re(1)-x			2.5073 (10)	2.162(3)	2.135(5)
Re(1)-N(3)			2.150(4)	2.168(4)	2.164(5)
Re(1)-N(1)			2.216(3)	2.207(4)	2.195(5)
O(2)-C(1)	1.215 (3)	1.248(2)	1.218(5)	1.237(5)	1.230(9)
O(1)-C(1)	1.292 (3)	1.271(2)	1.329(5)	1.255(5)	1.269(9)
N(1)-C(2)	1.299 (3)	1.293(2)	1.310(5)	1.297(5)	1.291(9)
N(2)-N(1)	1.357 (3)	1.368(2)	1.363(5)	1.377(5)	1.390(8)
N(3)-Re(1)-X			81.29 (10)	78.38(13)	81.87(20)
N(3)-Re(1)-N(1)			75.53 (13)	74.63(13)	74.80(21)
N(1)-Re(1)-X			81.19(9)	81.68(12)	77.81(20)
O(2)-C(1)-O(1)	125.2 (2)	124.82 (18)	122.2(4)	125.1(4)	129.0(7)
C(2)-N(1)-N(2)	119.5 (2)	119.35 (16)	120.0(4)	117.9(4)	116.7(5)
C(31)-N(2)-N(1)	119.2 (2)	116.60 (16)	120.2(4)	119.3(4)	118.6(6)

(a)Average values are included.

The Re-N_{py} distances in **1A**, **2B** and **1C** (Table 1) are slightly longer than for previously reported hydrazinopyridines [24,25].

The molecular structure of the dimer **2B** is presented in Fig. 3b. This compound crystalized in the triclinic centrosymmetric space group (*P*-1) and the asymmetric unit contains half of the centrosymmetric dimer $[Re_2(L^2)_2(CO)_6]$ and one methanol molecule. The deprotonated ligand L^2 coordinated to a rhenium atom by the N3 and N1 nitrogen atoms, forming a chelate ring analogous to that observed for **1A** (κ^2-N_{py},N), with the {Re(L^2)$(CO)_3$} entities being joined by carboxylate oxygen atoms. This coordination mode, μ-1κ^2-N_{py},N:2κO, changes the configuration of the N1-C1 bond to *E* breaking the intramolecular N2-H···O interaction observed in **HL^2** and **1A**. The carboxylate group, as well the phenol group at C2, are now almost orthogonal (86.98°) to the plane defined by the pyridine and hydrazone group. This arrangement of the phenol and carboxylate groups also allows the establishment of hydrogen interactions between dimers, in which the methanol molecule also plays a role by associating the complex in chains (Fig. 4, bottom).

In the structure of **1C**·2DMSO, the deprotonated ligand maintains the bidentate-bridge coordination mode observed in **2B**, i.e.: μ-1κ^2-N_{py}, N:2κO, although three {Re(L^1)$(CO)_3$} units are now associated. Again, this coordination mode places the carboxylate group on an almost orthogonal plane with respect to pyridinehydrazone group. The units forming the trimer are independent from the crystallographic point of view, but the differences in bond distances and angles are not significant. A differentiating aspect with respect to **2B** is that the trimer **1C** is formed by homochiral units (although both enantiomers are present in the crystal as evidenced the centrosymmetric nature of the crystal in the space group $P2_1/c$) and consequently, the three {Re$(CO)_3$} fragments possess carbonyl groups pointing in the same direction (Fig. 3d). This aspect differentiates it from other similar trimeric rhenium structures where the carbonyls are arranged with the maximum possible distance. [41].

The trimers are chained by C—H···O interactions between the phenyl and carbonyl groups in a head-to-tail style (Fig. 3d), while the solvent molecules (DMSO) are distributed around them by through N2-H···O_{DMSO} and other weak interactions (see Table S3). It is worth

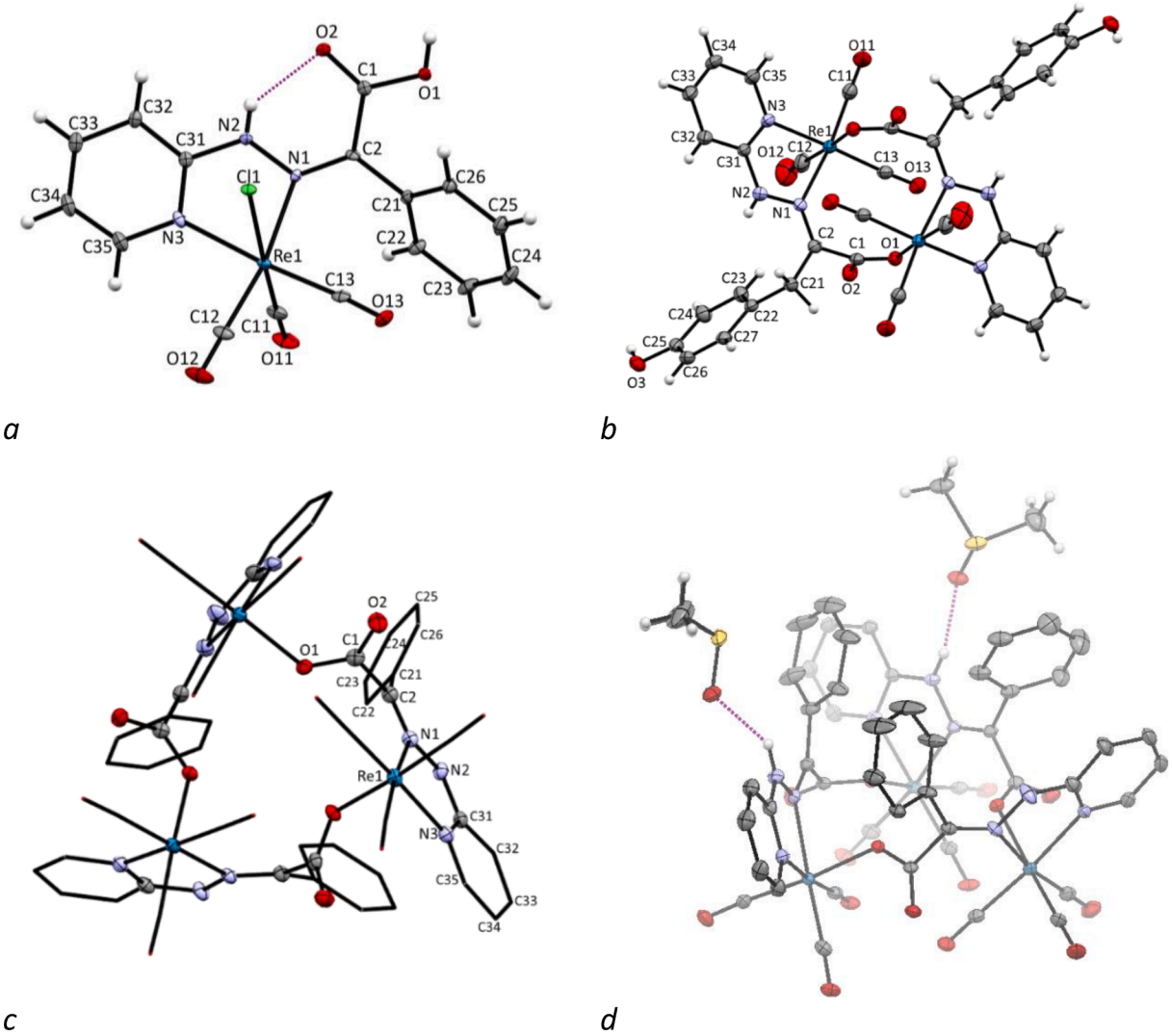

Fig. 3. Molecular structure of **1A** (a), **2B** (b) and **1C** (c,d). Solvent molecules were removed for clarity. In the case of **1C**, hydrogen atoms were also omitted and the ellipsoids are represented with the 25 % probability level.

mentioning that a third solvent molecule was removed with the SQUEEZE tool [42,43] due to its high disorder. Presumably, the resulting void corresponds to another DMSO (the results show two cavities of 728 $Å^3$ of 240 electrons each one), which would interact with ligand B in a manner analogous to the other DMSO molecules.

2.3. IR and theoretical study

The structures of **1A**, **2B** and **1C** were optimized by DFT using the X-ray diffraction data as starting points. From these structures, input geometries of **2A**, **1B** and **2C** were constructed. All DFT calculations used the hybrid wB97XD functional, which incorporates empirical dispersion corrections. Frequency calculations were subsequently performed to confirm the nature of the optimized geometries as stationary points and to obtain vibrational frequencies. The geometries calculated in the gas phase show only slight differences in the bond distances and angles when compared to the X-ray structures (see Table S4).

The theoretical calculations were carried out to gain information on the structure and nuclearity of the complexes investigated here, in particular those isolated as non-crystalline phases. Frequency calculations were found to be very useful for structure identification, notably by comparing the region of the IR spectrum of carbonyl ligands, since the intensity and relative positions of the bands are representative of the structure of the carbonyl complex (see Fig. 5). Recently, the study of these spectra allowed the characterization of the isomerization process in Mn_2S_2 diamond core-based complexes of tricarbonyl manganese(I) [44]. In our case, the spectra in the 1800–2100 cm^{-1} range, where carbonyl ligand stretching modes are expected, experience significant changes depending on whether the complexes are mono–, di– or tri-nuclear. This fact helps us to confirm, together with the rest of the characterization techniques, that the amorphous powder from which the **1C** crystal was obtained contains the same structure (*vide supra*).

The IR spectrum of **1A** displays three absorption bands at 2026, 1919 and 1890 cm^{-1}, with the latter showing a shoulder on the high energy side at 1916 cm^{-1}. The highest energy band is assigned to the symmetric stretching vibration of the carbonyl groups (ν_1), while the lowest energy band is attributed to the asymmetric stretch of the equatorial CO groups (ν_3). Finally, the shoulder at 1919 cm^{-1} is assigned to the asymmetric stretching vibration of the axial CO group (ν_2) [45,46]. The spectrum calculated with DFT reproduces quite well the shape of the experimental spectrum (Fig. 4), with the stretching vibration ν_2 having a lower intensity with respect to the asymmetric ones ν_3, which are very close in energy.

The three CO stretching vibrations are shifted to lower energies in the spectrum of **1C** compared with that of **1A**, being observed at 2020, 1912 and 1873 cm^{-1}. This shift is small for the symmetric vibration ν_1

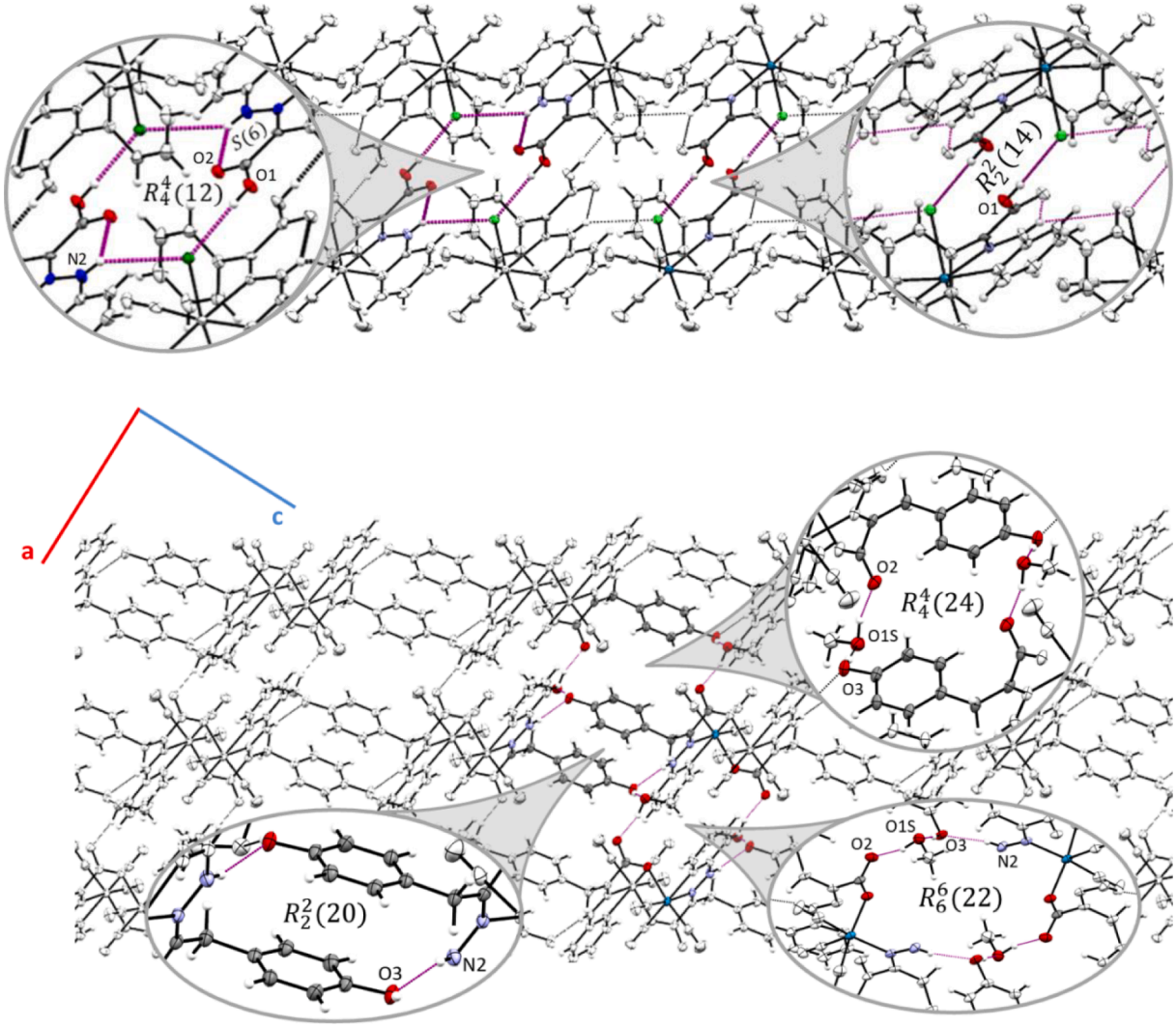

Fig. 4. Association by hydrogen bonding in the **1A** (top) and **2B**·2CH_3OH (bottom) crystals.

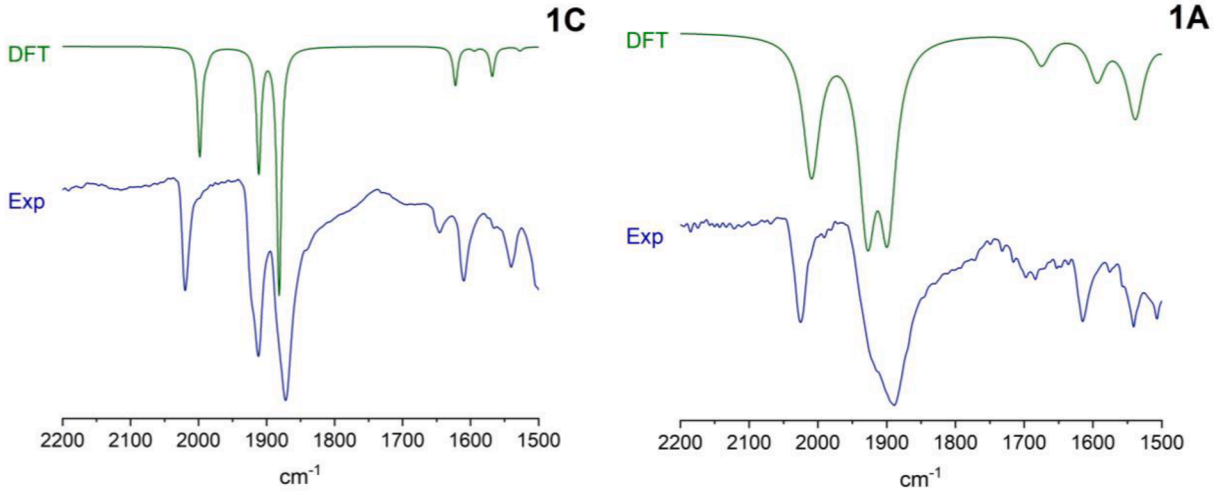

Fig. 5. Overlay of theoretical (top, linewidths of 14 cm^{-1}) and experimental (bottom) IR spectra of the non-crystalline solid phase obtained in the synthesis of **1C** (left) and **1A** (right). Wavenumbers in the theoretical spectra were scaled with a factor of 0.94.

(6 cm^{-1}) and the asymmetric vibration ν_2 (4 cm^{-1}), but more significant for the asymmetric vibration ν_3 (17 cm^{-1}). As a result, the two bands observed at lower energy are well-resolved in the experimental spectrum, a situation that is also evident in the spectrum calculated with DFT methods.

These results suggest that the reaction of $[ReCl(CH_3CN)_2(CO)_3]$ with the HL^1 ligand in the presence of a base yields a trinuclear complex whose structure is essentially that determined from the single crystal obtained from DMSO solutions (complex **1C**). The significant shift of the band associated to the asymmetric vibration of equatorial COs (ν_3) can be explained by the structure of the trinuclear complex described above, as these CO groups point to neighbouring $Re(L^1)(CO)_3$ units. Conversely, axial CO groups are pointing outwards, and thus the central CO stretching band is less affected upon formation of the trinuclear entity.

A second objective of the DFT study was to determine if there is any stabilizing effect that determines the systematic isolation of trinuclear complexes after deprotonation of the HL^1 ligand but not in the case of HL^2. For this purpose, we computed the Gibbs free energies at 298.15 K for equilibrium (1) (Scheme 4), which involves the dinuclear and trinuclear entities. These calculations used the geometries of complexes B (centrosymmetric dimer) and C (chiral trimer) minimized from those determined by X-ray diffraction.

The transformation of the dinuclear to the trinuclear complex is a spontaneous process with the deprotonated HL^1 ligand, while the equilibrium shifts to the formation of the dimeric structiore in the case of HL^2. These results agree with the detection of the presence of only trinuclear species when deprotonation of HL^1 is induced. In the case of HL^2, attempts have been made to obtain the trimeric complex by reproducing the synthesis of **1C** but were not able to isolate a structurally unique compound. Nevertheless, the data suggest the presence of the dinuclear compound **2B** as detected in the batch isolated as single crystals.

A multitude of dinuclear Re(I) species can be found in the literature. However, it is rare to find trinuclear [47] and much more trimeric structures, where the monomeric Re-L unit assembles to give the $\{Re_3L_3\}$ entity. This is normal considering that a lot of stress is generated in this type of geometries, for which is only observed with certain ligands (ATOHEW [48] or DEQKUG [49], for example). On the other hand, in our group we identified how when forming this type of discrete aggregates, the steric demands imposed by a substituent could limit the number of units to be assembled. This is the case of tetra- or trinuclear complexes formed by pyrazolone ligands derived from thiosemicarbazones and the fragment $\{Re(CO)_3\}$, where the nature of a substituent near the donor group resulted in four (H or Me) [50] or three (Ph) [49] assembled units. In the present case, the results suggest that the CH_2-Ph-OH substituent in the HL^2 ligand imposes greater steric demand than the phenyl group in HL^1.

3. Conclusions

In this work we have described two new hydrazone ligands derived from α-keto acids, as well as their behaviour towards the *fac*-$\{Re(CO)_3\}^+$ moiety. These zwitterionic compounds present a bidentate coordination mode through the pyridine and iminic groups, forming a five-membered chelate ring with rhenium. When the reaction is carried out in a neutral medium, the carboxylate does not participate in the coordination. However, if a base is used in the reaction, this group acts as a bridge between the metals, allowing the formation of di- or trinuclear species. Despite the structural similarities, we have been able to verify the number of units assembled in each case.

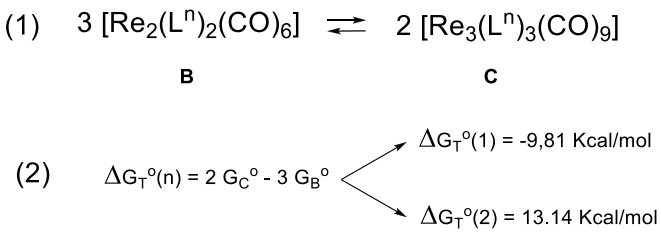

Scheme 4. Theoretical energies for the transformation of dinuclear and trinuclear complexes derived from $\mathbf{HL^1}$ (n = 1) and $\mathbf{HL^2}$ (n = 2).

4. Experimental section

4.1. Materials and physical measurements

The starting materials and solvents were obtained commercially and were used as supplied. The adduct $[ReCl(CH_3CN)_2(CO)_3]$ was synthesized following the methods of Farona and Kraus [51] from the $[ReCl(CO)_5]$ obtained following a similar method to that proposed by Schmidt [52].

Elemental analyses (C, H, N) were carried out using an elemental analysis Fisons Carlo Erba EA110. Mass spectra (ESI^+) were recorded using a micrOTOF-Focus and a SolariX XR (Bruker Daltonics) spectrometers. IR spectra were recorded in the solid phase by ATR (4000–400 cm^{-1}) using a Jasco FT/IR-6100 spectrophotometer. ^1H NMR spectra were obtained in DMSO-d_6 using a Bruker AVANCE 400 spectrometer.

4.2. Computational details

Optimizations of all systems were performed with the Gaussian 16 program package (revision C.01) [53], using the pseudopotential approximation and the wB97XD functional [54], which includes empirical dispersion. We selected the ECP60MDF relativistic pseudopotential of the Stuttgart/Cologne group (60 electrons in the core for Re) and the associated ECP60MDF_VTZ valence basis set for rhenium [55], while the Def2-TZVP basis set [56] was used for all other atoms. No restraints were imposed for geometry optimization, while frequency calculations were used to confirm the nature of the optimized geometries as stationary points. The size of the integration grid was increased with the integral = ultrafine keyword.

4.3. Crystallography

The crystallographic data were collected at 100 K using a Bruker D8 Venture diffractometer with a Photon 100 CMOS two-dimensional detector and Mo-Kα radiation (λ = 0.71073 Å) generated by an Incoatec high brillance microfocus source equipped with Incoatec Helios multilayer optics. The APEX3 software was used to collect frames of data, index reflections and determine the lattice parameters; SAINT was used for integration of the intensity of reflections and SADABS for scaling and empirical absorption correction [57]. The structures were solved using the SHELXT program [58]; all non-hydrogen atoms were refined on F^2 with anisotropic thermal parameters using SHELXL [59]. Hydrogen atoms were inserted at calculated positions and refined as riding atoms except those bonded to heteroatoms (N—H and O—H) which were generally located from the electron density synthesis Fo-Fc map and isotropically refined. Validation checking of the models (including for missed symmetry) and the used of SQUEEZE [42,43] tool was performed using PLATON and plots of all structures were produced using MERCURY [60] with a 50 % of thermal ellipsoid probability level, unless a different value is specified.

The crystallographic data collection and refinement parameters are listed in Table S1.

4.4. Synthesis of the complexes $[ReCl(CO)_3(HL^n)]$ (n = 1, 1A; n = 2, 2A)

A mixture of the rhenium precursor *fac*-$[ReCl(CH_3CN)_2(CO)_3]$ (0.25 mmol) and the corresponding ligand $HL^{1\text{-}2}$ (0.25 mmol) were refluxed in

methanol for 2.5 h. The resulting solution was vacuum concentrated after the addition of diethyl ether and chloroform, obtaining a dark solid which was collected by filtration and dried *in vacuo* over $CaCl_2$/KOH.

1A·$^1/_3$CHCl$_3$: Yield: 117 mg (83 %). M.p.: 199 °C. $C_{16}H_{11}ClN_3O_5Re \cdot {}^1/_3CHCl_3$ (586.30): calcd. C 33.4, H 1.9, N 7.2; found C 33.8, H 2.2, N 7.3 %. MS-ESI$^+$ [*m/z* (%)]: 512.02 (100) $|M-Cl|^+$, 553.05 (64) $|M-Cl + CH_3CN|^+$. IR (ATR, ν/cm^{-1}): 2025 s, 1889vs $\nu(C{\equiv}O)_{fac}$; 1614 m $\nu(CO_2)$; 1542 m, 1507 m, 1488 m $\nu(C{=}N)$.

^{1}H RMN (400 MHz, DMSO-d_6, ppm): Spectra shows two signal sets (' minority): 15.10 (s, 1H, N2H), 11.74 (s, 1H, O1H), 8.39 (d, ^3J = 5.8 Hz, 1H, C35H'), 8.35 (dd, ^3J = 5.7 Hz, ^4J = 0.6 Hz, 1H, C35H), 7.91 (ddd, ^3J = 8.7 Hz, ^3J = 7.4 Hz, ^4J = 1.5 Hz, 1H, C33H), 7.85 (ddd, ^3J = 8.7 Hz, ^3J = 7.4 Hz, ^4J = 1.5 Hz, 1H, C33H'), 7.65–7.62 (*m*, 1H, C22H, C26H), 7.60–7.57 (*m*, 1H, C22H', C26H'), 7.48–7.46 (*m*, 3H, C23H', C24H', C25H'), 7.46–7.44 (*m*, 3H, C23H, C24H, C25H), 7.42 (d, ^3J = 8.6 Hz, 1H, C32H), 7.19 (d, ^3J = 8.6 Hz, 1H, C32H'), 6.99 (ddd, ^3J = 7.2 Hz, ^3J = 5.9 Hz, ^4J = 1.0 Hz, 2H, C34H, C34H').

Single crystals of **1A** were obtained by slow evaporation of a solution of the powder in methanol at room temperature.

2A·H$_2$O: Yield: 113 mg (86 %). M.p.: 180 °C. $C_{17}H_{13}ClN_3O_6Re{\cdot}H_2O$ (594.98): calcd. C 34.3, H 2.5, N 7.1; found C 34.7, H 2.5, N 6.9 %. MS-ESI$^+$ [*m/z* (%)]: 272.10 (91) $|HL + H|^+$, 542.04 (56) $|M-Cl|^+$, 583.07 (100) $|M-Cl + CH_3CN|^+$. IR (ATR, ν/cm^{-1}): 3183b ν(OH/NH); 2023 s, 1885vs $\nu(C{\equiv}O)_{fac}$; 1612 s $\nu(CO_2)$; 1550 m, 1511 s, 1488 m $\nu(C{=}N)$.

^{1}H RMN (400 MHz, DMSO-d_6, ppm): Spectra shows two signal sets (' minority): 15.02 (s, 1H, N2H), 11.70 (s, 1H, O1H), 9.39 (s, 1H, O3H, O3H'), 8.36 (d, ^3J = 5.2 Hz, 1H, C35H, C35H'), 7.90 (ddd, ^3J = 8.7 Hz, ^3J = 7.3 Hz, ^4J = 1.6 Hz, 1H, C33H), 7.86 (ddd, ^3J = 8.6 Hz, ^3J = 7.0 Hz, ^4J = 1.6 Hz, 1H, C33H'), 7.29 (d, ^3J = 8.5 Hz, 1H, C32H), 7.26 (d, ^3J = 8.5 Hz, 1H, C32H'), 7.16 (d, ^3J = 8.5 Hz, 2H, C23H', C27H'), 7.11 (d, ^3J = 8.5 Hz, 2H, C23H, C27H), 6.99 (ddd, ^3J = 7.1 Hz, ^3J = 6.0 Hz, ^4J = 1.1 Hz, 1H, C34H), 6.96 (ddd, ^3J = 7.1 Hz, ^3J = 6.1 Hz, ^4J = 1.1 Hz, 1H, C34H'), 6.71 (d, ^3J = 8.6 Hz, 1H, C24H, C26H), 6.67 (d, ^3J = 8.6 Hz, 1H, C24H', C26H'), 4.25 (q, ^2J = 14.8 Hz, 2H, C21H'), 4.20 (d, ^2J = 17.1 Hz, 1H, C21Ha), 4.02 (d, ^2J = 17.1 Hz, 1H, C21Hb).

Single crystals of $[Re_2(L^2)_2(CO)_6]$, **2B**, were obtained by slow evaporation of a solution of **2A** in methanol at room temperature.

4.5. Synthesis of the complex $[Re_3(L^1)_3(CO)_9]$ (1C)

A mixture of the rhenium precursor *fac*-$[ReCl(CH_3CN)_2(CO)_3]$ (0.25 mmol) and the ligand HL^1 (0.25 mmol) with NEt_3 (0.25 mmol) were refluxed in THF (5 mL) for 3 h. The solid formed was filtered off, washing with water and dried *in vacuo* over $CaCl_2$/KOH.

1C·3H$_2$O: Yield: 61 mg (47 %). M.p.: 213 °C. $C_{48}H_{30}N_9O_{15}Re_3$ (1533.05): calcd. C 36.3, H 2.3, N 7.9; found C 36.1, H 2.3, N 7.9 %. MS-ESI$^+$ [*m/z* (%)]: 512.03 (100) $|M/3 + H|^+$, 553.05 (58) $|M/3 + CH_3CN + H|^+$, 1021.04 (16) $|M/2 + H|^+$, 1532.06 (2) $|M + H|^+$. IR (ATR, ν/cm^{-1}): 2651 ν(OH/NH); 2020 s, 1912 s, 1873vs $\nu(C{\equiv}O)_{fac}$; 1610 s $\nu(CO_2)$; 1541 m, 1497 s, 1443 m $\nu(C{=}N)$.

^{1}H RMN (400 MHz, DMSO-d_6, ppm): 8.26 (ddd, ^3J = 5.8 Hz, ^4J = 1.5 Hz, ^4J = 0.7 Hz, 1H, C35H), 7.79 (ddd, ^3J = 8.7 Hz, ^3J = 7.2 Hz, ^4J = 1.6 Hz, 1H, C33H), 7.39–7.37 (*m*, 3H, C22H, C26H, C24H), 7.36–7.32 (*m*, 2H, C23H, C25H), 7.20 (d, ^3J = 8.5 Hz, 1H, C32H), 6.83 (ddd, ^3J = 7.0 Hz, ^3J = 6.0 Hz, ^4J = 1.0 Hz, 1H, C34H).

Single crystals of **1C** were obtained by the slow evaporation of a solution of the compound in DMSO-d_6 at room temperature.

The same structure was again obtained by recrystallization in DMSO of the reaction crude between stoichiometric amounts of **HL^1** and $[ReCl(CO)_5]$ in boiling toluene.

CRediT authorship contribution statement

Aida Lorenzo: Formal analysis, Investigation. **Saray Argibay-Otero:** Formal analysis, Investigation, Writing – original draft, Writing – review & editing. **Carlos Platas-Iglesias:** Formal analysis, Writing – review & editing. **Ezequiel M. Vázquez-López:** Formal analysis, Project administration, Writing – review & editing.

Declaration of competing interest

The authors declare that they have no known competing financial interests or personal relationships that could have appeared to influence the work reported in this paper.

Data availability

Data will be made available on request.

Acknowledgments

Financial support from the Ministerio de Ciencia e Innovación (Spain) under research projects PID2019-110218RB-I00 and RED2022-134091-T is gratefully acknowledged. We thank the Structural Determination Service of the Universidade de Vigo-CACTI for X-ray diffraction measurements.

Funding for open access charge: Universidade de Vigo/CISUG.

Appendix A. Supplementary data

CCDC-2297244, CCDC-2297264, CCDC-2297380, CCDC-2297397 and CCDC-2298789 (see Table S1) contain the supplementary crystallographic data for this paper. These data can be obtained free of charge via http://www.ccdc.cam.ac.uk/conts/retrieving.html, or from the Cambridge Crystallographic Data Centre, 12 Union Road, Cambridge CB2 1EZ, UK; fax: (+44) 1223-336-033; or e-mail: deposit@ccdc.cam.ac.uk. Supplementary data to this article can be found online at https://doi.org/10.1016/j.poly.2023.116789.

References

[1] L.R. Gray, S.C. Tompkins, E.B. Taylor, Regulation of pyruvate metabolism and human disease, Cell. Mol. Life Sci. 71 (2014) 2577, https://doi.org/10.1007/s00018-013-1539-2.
[2] A. Lopalco, J. Douglas, N. Denora, V.J. Stella, Determination of pKa and Hydration Constants for a Series of α-Keto-Carboxylic Acids Using Nuclear Magnetic Resonance Spectrometry, J. Pharm. Sci. 105 (2) (2016) 664, https://doi.org/10.1002/jps.24539.
[3] U. Rüetschi, R. Cerone, C. Pérez-Cerda, M.C. Schiaffino, S. Standing, M. Ugarte, E. Holme, Mutations in the 4-hydroxyphenylpyruvate dioxygenase gene (HPD) in patients with tyrosinemia type III, Hum. Genet. 106 (6) (2000) 654, https://doi.org/10.1007/s004390000307.
[4] L. Cassidei, A. Dell'Atti, O. Sciacovelli, A Spectroscopic Study on p-Hydroxyphenylpyruvic Acid. Keto-Enol Tautomerism and Stability of Its Complex with Fe+3 Ions, Z. Naturforsch. C 35 (1980) 1, https://doi.org/10.1515/znc-1980-1-202.
[5] F.J. van Spronsen, N. Blau, C. Harding, A. Burlina, N. Longo, A.M. Bosch, Phenylketonuria, Nat. Rev. Dis. Primers 7 (1) (2021) 36, https://doi.org/10.1038/s41572-021-00267-0.
[6] Terre'Blanche, G., Heyer, N., Bergh, J. J., Mienie, L. J., van der Schyf, C. J., Harvey, B. H., The Styrene Metabolite, Phenylglyoxylic Acid, Induces Striatal-Motor Toxicity in the Rat: Influence of Dose Escalation/Reduction over Time Neurotox Res, 2011, 20, 97. doi: 10.1007/s12640-010-9222-y.
[7] P. Jia, L. Gao, Y. Zheng, X. Zheng, C. Wang, C. Yang, Y. Li, Y. Zhao, Ultrastable Tb-Organic Framework as a Selective Sensor of Phenylglyoxylic Acid in Urine, ACS Appl. Mater. Interfaces 13 (2021) 33546, https://doi.org/10.1021/acsami.1c09202.
[8] T.N. Sorrell, Organic Chemistry 2Ed, University Science Books, California, 2006.
[9] H. Qian, I. Aprahamian, An emissive and pH switchable hydrazone-based hydrogel, Chem. Commun. 51 (2015) 11158, https://doi.org/10.1039/c5cc03007b.
[10] B. Begovic, S. Ahmedtagic, L. Calkic, M. Vehabovic, S.B. Kovacevic, T. Catic, M. Mehic, Open Clinical Trial on Using Nifuroxazide Compared to Probiotics in Treating Acute Diarrhoeas in Adults, Mater. Sociomed. 28 (2016) 454, https://doi.org/10.5455/msm.2016.28.454-458.
[11] C.M. Clark, D.F. Elmendorf, W.U. Cauthon, C. Muschenheim, W. McDermott, Isoniazid (isonicotinic acid hydrazide) in the treatment of miliary and meningeal tuberculosis, Am. Rev. Tuberc. 66 (1952) 391.
[12] I. Iliev, D. Kontrec, R. Detcheva, M. Georgieva, A. Balacheva, N. Galic, T. Pajpanova, Cancer cell growth inhibition by aroylhydrazone derivatives, Biotechnol. Biotec. Eq. 33 (2019) 756, https://doi.org/10.1080/13102818.2019.1608302.

[13] P. Dandawate, E. Khan, S. Padhye, H. Gaba, S. Sinha, J. DeshpandeK, V. Swamy, M. Khetmalas, A. Ahmad, F.H. Sarkar, Synthesis, characterization, molecular docking and cytotoxic activity of novel plumbagin hydrazones against breast cancer cells, Bioorg. Med. Chem. Lett. 22 (2012) 3104, https://doi.org/10.1016/j.bmcl.2012.03.060.

[14] J. Patole, U. Sandbhor, S. Padhye, D.N. Deobagkar, C.E. Anson, A. Powell, Structural chemistry and In vitro antitubercular activity of acetylpyridine benzoyl hydrazone and its copper complex against Mycobacterium smegmatis, Bioorg. Med. Chem. Lett. 13 (2003) 51, https://doi.org/10.1016/s0960-894x(02)00855-7.

[15] I. Babahan, E.P. Coban, H. Biyik, Synthesis, characterisation and antimicrobial activities of vic-dioxime derivatives containing heteroaromatic hydrazone groups and their metal complexes, Maejo Int. J. Sci. Technol. 7 (2013) 26, https://doi.org/10.14456/mijst.2013.2.

[16] P. Barbazán, R. Carballo, B. Covelo, C. Lodeiro, J.C. Lima, E.M. Vázquez-López, Synthesis, Characterization, and Photophysical Properties of 2-Hydroxybenzaldehyde [(1E)-1-pyridin-2-ylethylidene]hydrazone and Its Rhenium(I) Complexes, Eur. Inorg. Chem. 2008 (17) (2008) 2713, https://doi.org/10.1002/ejic.200701199.

[17] I. Picón-Ferrer, F. Hueso-Ureña, N.A. Illán-Cabeza, S.B. Jiménez-Pulido, J. M. Martínez-Martos, M.J. Ramírez-Expósito, M.N. Moreno-Carretero, Chloro-fac-tricarbonylrhenium(I) complexes of asymmetric azines derived from 6-acetyl-1,3,7-trimethylpteridine-2,4(1H,3H)-dione with hydrazine and aromatic aldehydes: Preparation, structural characterization and biological activity against several human tumor cell lines, J. Inorg. Biochem. 103 (2009) 94, https://doi.org/10.1016/j.jinorgbio.2008.09.014.

[18] R. Alberto, The particular role of radiopharmacy within bioorganometallic chemistry, J. Organomet. Chem. 692 (2007) 1179, https://doi.org/10.1016/j.jorganchem.2006.11.019.

[19] J. Grewe, A. Hagenbach, B. Stromburg, R. Alberto, E.M. Vázquez-López, Abram, U, Tricarbonyl Complexes of Rhenium(I) with Acetylpyridine Benzoylhydrazone and Related Ligands, Z. Anorg. Allg. Chem. 629 (2003) 303, https://doi.org/10.1002/zaac.200390048.

[20] M. Emami, H. Shahroosvand, R. Bikas, T. Lis, C. Daneluik, M. Pilkington, Synthesis, Study, and Application of Pd(II) Hydrazone Complexes as the Emissive Components of Single-Layer Light-Emitting Electrochemical Cells, Inorg. Chem. 60 (2021) 982, https://doi.org/10.1021/acs.inorgchem.0c03102.

[21] T. Ramesh, B. Bryant, T. Nayak, C.M. Revankar, T. Anderson, K.E. Carlson, J. A. Katzenellenbogen, L.A. Sklar, J.P. Norenberg, E.R. Prossnitz, J.B. Arterburn, Linkage Effects on Binding Affinity and Activation of GPR30 and Estrogen Receptors ERα/β with Tridentate Pyridin-2-yl Hydrazine Tricarbonyl−Re/99mTc (I) Chelates, J. Am. Chem. Soc. 128 (2006) 14476, https://doi.org/10.1021/ja066360p.

[22] P. Barbazán, A. Hagenbach, E. Oehlke, U. Abram, R. Carballo, S. Rodríguez-Hermida, E.M. Vázquez-López, Tricarbonyl Rhenium(I) and Technetium(I) Complexes with Hydrazones Derived from 4,5-Diazafluoren-9-one and 1,10-Phenanthroline-5,6-dione, Eur. J. Inorg. Chem. 2010 (29) (2010) 4622, https://doi.org/10.1002/ejic.201000522.

[23] Y. Pocker, J.E. Meany, B.J. Nist, C. Zadorojny, Reversible hydration of pyruvic acid. I. Equilibrium Studies, J. Phys. Chem. 73 (9) (1969) 2879, https://doi.org/10.1021/j100843a015.

[24] P. Barbazán, R. Carballo, I. Prieto, M. Turnes, E.M. Vázquez-López, Synthesis and characterization of several rhenium(I) complexes of 2-acetylpyridine and ferrocenyl carbaldehyde derivatives of 2-hydroxybenzoic acid hydrazide, J. Organomet. Chem. 694 (19) (2009) 3102, https://doi.org/10.1016/j.jorganchem.2009.05.032.

[25] S. Argibay, D. Costas-Riveiro, R. Carballo, E.M. Vázquez-López, Coordination modes of hydrazone and acyl-hydrazone ligands containing a pyridine group with the {Re(CO)3}+ fragment, Polyhedron 222 (2022), 115917, https://doi.org/10.1016/j.poly.2022.115917.

[26] S. Argibay, A.M. Graña, R. Carballo, E.M. Vázquez-López, Synthesis of Novel Dinuclear N-Substituted 4-(Dimethylamino)benzaldehyde Thiosemicarbazonates of Rhenium(I): Formation of Four- and/or Five-Membered Chelate Rings, Conformational Analysis, and Reactivity, Inorg. Chem. 59 (19) (2020) 14101, https://doi.org/10.1021/acs.inorgchem.0c01887.

[27] A. Pino-Cuevas, A. Graña, U. Abram, R. Carballo, E.M. Vázquez-López, Structural study of mono-, di- and tetranuclear complexes of the {Re(CO)3}+ fragment with thiosemicarbazone/thiosemicarbazonate ligands containing benzothiazole or benzoxazole groups, CrystEngComm 20 (2018) 4781, https://doi.org/10.1039/C8CE00874D.

[28] Q. Feng, Z. Liu, L. Xiong, M. Wang, Y. Li, Z. Li, Synthesis and Insecticidal Activities of Novel Anthranilic Diamides Containing Modified N-Pyridylpyrazoles, J. Agric. Food Chem. 58 (2010) 12327, https://doi.org/10.1021/jf102842r.

[29] M.A. Affan, I.P.P. Foo, B.A. Fasihuddin, M.A. Hapipah, M. Shamsuddin, Synthesis, characterization and X-ray single crystal studies of mono-n-butyltin(IV) dichloride complex of pyruvic acid-2-pyridylhydrazone [n-BuSnCl2(PAP)], Indian J. Chem. 48A (2009) 1388.

[30] N. Filipovic, H. Borrmann, T. Todorovic, M. Borna, V. Spasojevic, D. Sladic, I. Novakovic, K. Andjelkovic, Copper(II) complexes of N-heteroaromatic hydrazones: Synthesis, X-ray structure, magnetic behavior, and antibacterial activity, Inorg. Chim. Acta 362 (6) (2009) 1996, https://doi.org/10.1016/j.ica.2008.09.019.

[31] T. Todorovic, S. Grubisic, M. Pregelj, M. Jagodic, S. Misirlic-Dencic, M. Dulovic, I. Markovic, O. Klisuric, A. Malesevic, D. Mitic, K. Andelkovic, N. Filipovic, Structural, Magnetic, DFT, and Biological Studies of Mononuclear and Dinuclear CuII Complexes with Bidentate N-Heteroaromatic Schiff Base Ligands, Eur. J. Inorg. Chem. 2015 (23) (2015) 3921, https://doi.org/10.1002/ejic.201500349.

[32] N. Filipovic, T. Todorovic, D. Radanovic, V. Divjakovic, R. Markovic, I. Pajic, K. Andjelkovic, Solid state and solution structures of Cd(II) complexes with two N-heteroaromatic Schiff bases containing ester groups, Polyhedron 31 (1) (2012) 19, https://doi.org/10.1016/j.poly.2011.07.023.

[33] S. Bjelogrlic, T.R. Todorovic, I. Cvijetic, M.V. Rodic, M. Vujcic, S. Markovic, J. Araskov, B. Janovic, F. Emhemmed, C.D. Muller, N.R. Filipovic, A novel binuclear hydrazone-based Cd(II) complex is a strong pro-apoptotic inducer with significant activity against 2D and 3D pancreatic cancer stem cells, J. Inorg. Biochem. 190 (2019) 45, https://doi.org/10.1016/j.jinorgbio.2018.10.002.

[34] N.R. Filipovic, A. Bacchi, G. Pelizzi, R. Markovic, D. Mitic, K.K. Andelkovic, Cobalt (III), zinc(II), cadmium(II) and palladium(II) complexes with the hydrolysed and non-hydrolysed condensation products of 2-acetylpyridine with ethyl hydrazinoacetate: X-ray structure analysis of mer-bis{(E)-2-[N′-(1-pyridin-2-yl-ethylidene)hydrazino] acetato}cobalt(III) tetrafluoroborate, J. Coord. Chem. 58 (2005) 1541, https://doi.org/10.1080/00958970500240383.

[35] N. Filipovic, M. Borna, O. Klisuric, M. Pregelj, M. Jagodic, K. Andelkovic, T. Todorovic, Synthesis, characterization, and thermal behavior of Cu(II) and Zn (II) complexes with (E)-2-[N′-(1-pyridin-2-yl-ethylidene)hydrazino]acetic acid (aphaOH). Crystal structure of [Zn2(aphaO)2Cl2], J. Coord. Chem. 66 (2013) 1549, https://doi.org/10.1080/00958972.2013.78605236.

[36] M.C. Etter, Encoding and decoding hydrogen-bond patterns of organic compounds, Acc. Chem. Res. 23 (1990) 120, https://doi.org/10.1021/ar00172a005.

[37] G.Giorgi, F.Ponticelli, L.Savini, L.Chiasserini, C.Pellerano, On the isomerism/tautomerism of hydrazones. Crystal structures, study in solution and theoretical calculations of new series of α-N-heterocyclic hydrazones J. Chem. Soc., Perkin Trans.2, 2000, 2000 (11), 2259. doi: 10.1039/b004448m.

[38] R. Melnicky, M. Grepl, A. Lycka, d, V. Bertolasi, L. Kvapil, B. Dvorakova, P. Hradil, The Preparation of Various New Heterocyclic Compounds via Cyclization of Substituted Derivatives of Phenacyl Esters of Hydrazonoacetic Acid Synthesis, 2013, 45 (17), 2447. doi: 10.1055/s-0033-1339348.

[39] P. Barbazán, R. Carballo, U. Abram, G. Pereiras-Gabián, E.M. Vázquez-López, Synthesis and characterization of ferrocenylcarbaldehyde benzoylhydrazone and its rhenium(I) complex, Polyhedron 25 (17) (2006) 3343, https://doi.org/10.1016/j.poly.2006.06.007.

[40] A. Hasheminasab, H.M. Rhoda, L.A. Crandall, J.T. Ayers, V.N. Nemykin, R. S. Herrick, C.J. Ziegler, Hydrazine-mediated strongly coupled Re(CO)3 dimers, Dalton Trans. 44 (2015) 17268, https://doi.org/10.1039/C5DT02821C.

[41] F. Zobi, B. Spingler, R. Alberto, Guanine and Plasmid DNA binding of Mono-and Trinuclear fac-[Re(CO)3]+ Complexes with Amino Acid Ligands, ChemBioChem 6 (2005) 1397, https://doi.org/10.1002/cbic.200400453.

[42] A.L. Spek, PLATON SQUEEZE: a tool for the calculation of the disordered solvent contribution to the calculated structure factors, Acta Crystallogr. C 71 (2015) 9, https://doi.org/10.1107/S2053229614024929.

[43] A.L. Spek, Structure validation in chemical crystallography, Acta Crystallogr. D 65 (2009) 148, https://doi.org/10.1107/S090744490804362X.

[44] T.H. Le, H. Nguyen, H.E. Arnold, D.J. Darensbourg, M.Y. Darensbourg, Chirality-Guided Isomerization of Mn2S2 Diamond Core Complexes: A Mechanistic Study, Inorg. Chem. 61 (41) (2022) 16405, https://doi.org/10.1021/acs.inorgchem.2c02460.

[45] K.T. Oppelt, L. Sevéry, M. Utters, S.D. Tilley, P. Hamm, Flexible to rigid: IR spectroscopic investigation of a rhenium-tricarbonyl-complex at a buried interface, Phys. Chem. Chem. Phys. 23 (2021) 4311, https://doi.org/10.1039/D0CP06546C.

[46] J.B. Asbury, W. Yongqiang, L. Tianquan, Time-Dependent Vibration Stokes Shift during Solvation: Experiment and Theory, Bull. Chem. Soc. Jpn. 75 (2002) 973, https://doi.org/10.1246/bcsj.75.973.

[47] S. Argibay, R. Carballo, E.M. Vázquez-López, Coordination Chemistry of Potentially S, N, Npy-Tridentate Thiosemicarbazones with the {Re(CO)3}+ Fragment and Formation of Hemiaminal Derivatives, Inorg. Chem. 62 (2023) 224, https://doi.org/10.1021/acs.inorgchem.2c03259.

[48] T. Brasey, A. Buryak, R. Scopelliti, K. Severin, Synthesis of a Metallamacrocyclic Re (CO)3 Complex Using a Tridentate Bridging Ligand, Eur. J. Inorg. Chem. 2004 (5) (2004) 964, https://doi.org/10.1002/ejic.200300880.

[49] P. Barbazán, R. Carballo, J.S. Casas, E. Garcia-Martinez, G. Pereiras-Gabian, A. Sanchez, E.M. Vazquez-Lopez, Synthesis and Characterization of New Trimeric Rhenium(I) Complexes. The Influence of Steric Factors on the Size of Pyrazolonaterhenium(I) Metallomacrocycles, Inorg. Chem. 45 (8) (2006) 7323, https://doi.org/10.1021/ic061080w.

[50] R. Carballo, J. Casas, E. García-Martínez, G. Pereiras-Gabián, A. Sánchez, J. Sordo, E.M. Vázquez-López, Rhenium(I)-Induced Cyclization of Thiosemicarbazones Derived from β-Keto Esters, Inorg. Chem. 42 (20) (2003) 6395, https://doi.org/10.1021/ic030154q.

[51] M.F. Farona, K.F. Kraus, Coordination of organonitriles through CN.pi. systems, Inorg. Chem. 9 (1970) 1700, https://doi.org/10.1021/ic50089a018.

[52] Schmidt, P., Trogler, W.C., Basolo, F., Inorganic Syntheses (Vol.28): Reagents for Transition Metal Complex and Organometallic Syntheses, J. Wiley & Sons, New York, 1990, pp. 160 –165.

[53] Frisch, M. J., Trucks, G. W., Schlegel, H. B., Scuseria, G. E., Robb, M. A., Cheeseman, J. R., Scalmani, G., Barone, V., Petersson, G. A., Nakatsuji, H., Li, X., Caricato, M., Marenich, A. V., Bloino, J., Janesko, B. G., Gomperts, R., Mennucci, B., Hratchian, H. P., Ortiz, J. V., Izmaylov, A. F., Sonnenberg, J. L., Williams-Young, D., Ding, F., Lipparini, F., Egidi, F., Goings, J., Peng, B., Petrone, A., Henderson, T., Ranasinghe, D., Zakrzewski, V. G., Gao, J., Rega, N., Zheng, G., Liang, W., Hada, M., Ehara, M., Toyota, K., Fukuda, R., Hasegawa, J., Ishida, M., Nakajima, T., Honda, Y., Kitao, O., Nakai, H., Vreven, T., Throssell, K., Montgomery, J. A., Peralta, J. E., F. Ogliaro, Bearpark, M. J., Heyd, J. J., Brothers, E. N., Kudin, K. N., Staroverov, V. N., Keith, T. A., Kobayashi, R., Normand, J.,

Raghavachari, A. P. Rendell, J. C. Burant, S. S. Iyengar, J. Tomasi, M. Cossi, J. M. Millam, M. Klene, C. Adamo, R. Cammi, J. W. Ochterski, K., Martin, R. L., Morokuma, K., Farkas, O., Foresman, J. B., Fox, D. J., Gaussian, Inc., Wallingford CT, 2016.

[54] J.D. Chai, M. Head-Gordon, Long-range corrected hybrid density functionals with damped atom–atom dispersion corrections, Phys. Chem. Chem. Phys. 10 (2008) 6615, https://doi.org/10.1039/B810189B.

[55] D. Figgen, K.A. Peterson, M. Dolg, H. Stoll, Energy-consistent pseudopotentials and correlation consistent basis sets for the 5d elements Hf–Pt, J. Chem. Phys. 130 (2009), 164108, https://doi.org/10.1063/1.3119665.

[56] F. Weigend, R. Ahlrichs, Balanced basis sets of split valence, triple zeta valence and quadruple zeta valence quality for H to Rn: Design and assessment of accuracy, Phys. Chem. Chem. Phys. 7 (18) (2005) 3297, https://doi.org/10.1039/B508541A.

[57] Bruker. APEX3, SAINT and SADABS. Bruker AXS Inc, Madison, Wisconsin, USA, 2015.

[58] Sheldrick, G.M., SHELXT - Integrated space-group and crystal-structure determination Acta Crystallogr A, 2015, 71, 3. doi: 10.1107/S2053273314026370.

[59] G.M. Sheldrick, A short history of SHELX, Acta Crystallogr. A 64 (2008) 112, https://doi.org/10.1107/S0108767307043930.

[60] C.F. Macrae, P.R. Edgington, P. McCabe, E. Pidcock, G.P. Shields, R. Taylor, M. Towler, J. van de Streek, Mercury: visualization and analysis of crystal structures, J. Appl. Cryst. 39 (2006) 453, https://doi.org/10.1107/S002188980600731X.